PrandtlPlane wing-box least-weight design: a multi-scale optimisation approach

Marco Picchi Scardaoni[a,b], Marco Montemurro[b,*], Enrico Panettieri[b]

[a] *University of Pisa, Department of Civil and Industrial Engineering, Aerospace division, via G. Caruso 8, 56122 Pisa, Italy*

[b] *Arts et Métiers Institute of Technology, Université de Bordeaux, CNRS, INRA, Bordeaux INP, HESAM Université, I2M UMR 5295, F-33405 Talence, France*

Abstract

The PrandtlPlane (PrP) aircraft wing-box least-weight design is presented in this work. This design problem is formulated as a constrained non-linear programming problem (CNLPP), by integrating static, buckling, fatigue and manufacturability requirements, under different loading conditions. The solution search is carried out by means of a suitable multi-scale optimisation (MSO) approach. The physical responses involved into the CNLPP formulation are evaluated at the wing-box architecture level (macroscopic scale) and at the stiffened panel level (component scale), as well. The scale transition is ensured by means of a suitable global-local (GL) modelling approach, while the CNLPP is solved by means of an in-house genetic algorithm. The effectiveness of the proposed approach is tested on the PrP wing-box structure, but the presented strategy can be easily extended to conventional aircraft wings.

Keywords: PrandtlPlane, Aircraft, Optimisation, Wing-box, Thin-walled structures, Genetic Algorithms

This is a pre-print of an article published in *Aerospace Science and Technology*.

The final authenticated version is available online at:

https://doi.org/10.1016/j.ast.2020.106156

*Corresponding author

Email address: marco.montemurro@ensam.eu, marco.montemurro@u-bordeaux.fr (Marco Montemurro)

1. Introduction

The PrandtlPlane (PrP) configuration, shown in Fig. 1, is the engineering application of the so-called "Best Wing System", introduced by L. Prandtl [1]: he theorised the existence of a lifting system which, for given wingspan and generated lift, minimises the induced drag. A rigorous mathematical proof of the Prandtl's riddle has been provided many years later [2].

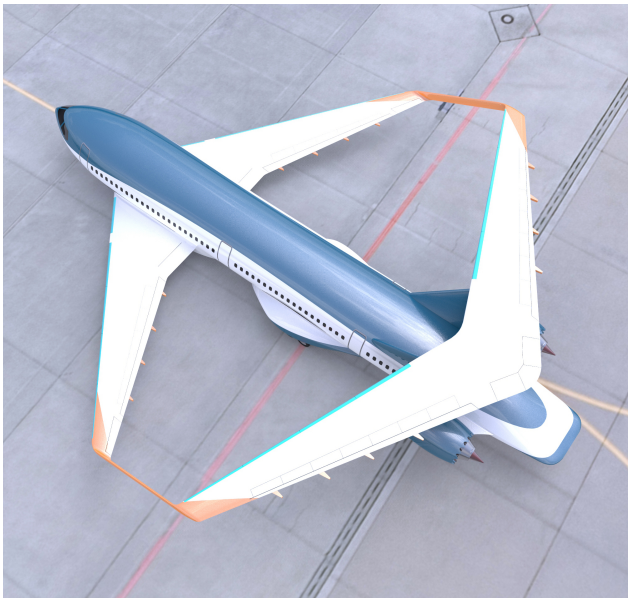

Figure 1: PrandtlPlane PARSIFAL MS1 rendering

Although the literature about aerodynamics of the PrP configuration is quite rich, there are few works focusing on the structural analysis, especially for the wing structure. The only works on this topic consider a now-obsolete PrP configuration and low-fidelity models [3–5]. Recently, a Finite Element (FE)-based approach for structural analysis of the PrP wing architecture has been proposed in [6], but the analysis was still carried out on an obsolete configuration of the wing. Moreover, a structural optimisation of the spars of an ultra-light PrP seaplane has been recently presented in [7, 8]. Paradoxically, in the literature there are more works about PrP aeroelasticity aspects (including non-linear ones) [4, 9–13], than works focusing on general structural behaviour of the PrP.

The structural analysis of the PrP aircraft architecture presents many features which make it quite challenging, if compared to a conventional aircraft. Unlike a conventional aircraft architecture, the PrP fuselage and lifting system form an hyperstatic structure.

Therefore, from a theoretical point of view, the structural problem should be faced as a whole. On the contrary, for conventional aircraft, one may separate the fuselage from the wing, the latter roughly considered as a "cantilever beam". This issue implies some important consequences. Firstly, one cannot separately deal with the structural analysis of the fuselage and the lifting system. Secondly, even if under some simplifying hypotheses it is possible to separate the structural analysis of the lifting system from that of the fuselage, the question about the complexity of the FE analysis still remains open. In this case, the complexity of the FE analysis should be intended in terms of model size, i.e. number of degrees of freedom (DOFs), compromise between accuracy and computational cost, choice of the scales of the analysis, choice of the design variables, etc. In this background, the need for suitable global-local (GL) modelling strategies, which may be a reasonable compromise between results accuracy and reduced computational costs, coupled to an efficient optimisation algorithm is of paramount importance.

Although [14] represents a recent exhaustive overview on methods for estimating lifting systems mass, authors do not cite GL approaches. Indeed, the vast majority of studies dealing with the structural analysis of (conventional) wing-box architectures for preliminary design purposes do not take into account GL approaches [15–17]. This is manly due to the important computational effort required to perform scale transition between global and local models which is often not compatible with the overall time required to perform the optimisation process [18]. However, as far as the development of GL strategies for the structural analysis of the lifting system of standard aircraft is concerned, some works can be found in the literature.

In [19], authors develop a GL strategy dedicated to Damage Tolerance analyses (DTAs), for conventional wings. Of course, DTAs needs a refined models of structural components in order to simulate cracks grow. This represents a first example of the need of changing structural scale in optimisation procedures. A more complete approach is presented in [20]. The global model does not take into account stringers and spar-cap, since stiffened panels are modelled as equivalent shells. Furthermore, only continuous variables are considered, which allow authors to use gradient-based techniques for the solution search. In [21] a GL strategy for a high-speed wing is presented . The main issue is that local models are re-mapped to rectangular plane stiffened plates, loosing geometry effects on instability

failures. Furthermore, several constraints are evaluated using analytical formula. In [22], the same authors extend the GL approach for the topology optimisation; nevertheless, the aforementioned issues remain. More recently, [23] presents a GL framework for optimisation of curvilinear spars and ribs (SpaRibs). The problem formulation presents a huge issue on computational cost: the framework needs hundreds of software licences and hundreds of cores to find solutions in acceptable time. Finally, in [24], authors extend the GL approach for a composite material simple wing, in the framework of the Carrera Unified Formulation (CUF).

As it can be inferred from this literature survey, GL modelling strategies are quite commonly used in the structural analysis of the wing-box structure of conventional aircraft. However, such strategies are rarely coupled to optimisation methods due to three main issues: (a) the high computational costs related to such an approach; (b) the lack of pertinent criteria to identify the zones of interest (ZOIs) within the global FE model (GFEM); (c) the lack of suitable modelling strategies to automatically build the local FE models (LFEMs) by extracting pertinent information from the GFEM and by taking into account for variable geometry and mesh.

In this scenario, a multi-scale optimisation (MSO) approach integrating an efficient GL modelling strategy [25–27] to evaluate all the necessary structural responses (at each pertinent scale) is applied to the PrP lifting system. The least-weight design of the PrP wing-box is stated as a classical constrained non-linear programming problem (CNLPP). The physical responses, evaluated by means of both GFEM and LFEMs, are integrated into the CNLPP formulation as optimisation constraints. The exchange between GFEM and LFEMs and the extraction of LFEMs from the GFEM are realised in a completely automatic way, without the user's intervention. The solution search for the CNLPP at hand is carried out by means of the ERASMUS (EvolutionaRy Algorithm for optimiSation of ModUlar Systems) algorithm developed by Montemurro [28], which is a special genetic algorithm (GA) able to deal with CNLPPs characterised by a variable number of design variables. This GA has been successfully used in other real-world engineering problems [29–39].

The paper is structured as follows. In Section 2 the design problem is presented together with the main hypotheses and the determination of the most relevant loading

conditions. Section 3 is dedicated to the mathematical formulation of the problem: optimisation variables are introduced and constraints discussed. Some details about the numerical strategy are also presented. Section 4 presents the adopted GL modelling strategy by putting the accent on the details for automatically identifying and extracting the ZOI. Section 5 discusses the numerical results, whilst Section 6 ends the paper with some meaningful conclusions and perspectives.

2. Least-weight design of a PrandtlPlane wing-box: problem description

The PrP lifting system considered in this work is the result of a preliminary aerodynamic study presented in [40, 41]. The PrP lifting system can be ideally split into three (semi-)wings: the front wing (FW), the rear wing (RW) and the vertical wing (VW), as shown in Fig. 2. In the same picture, the global Body reference frame $\mathcal{T}_B(\mathrm{CG}; X_B, Y_B, Z_B)$, centred at the aircraft center of mass (CG), is illustrated.

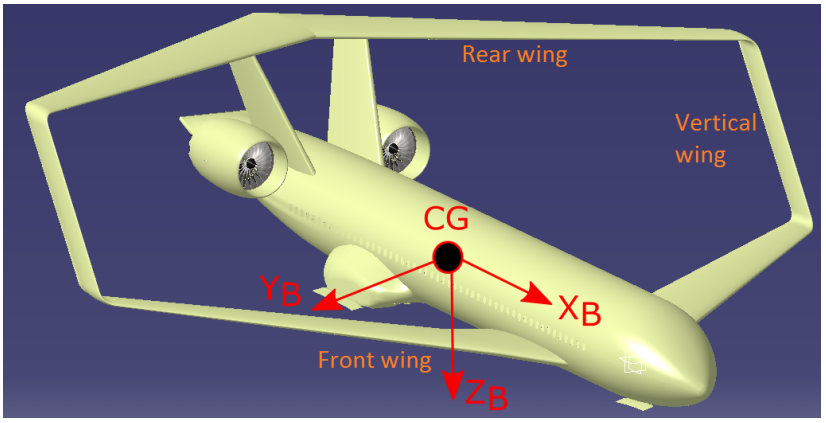

Figure 2: PrP aircraft rendering

Due to the symmetry of the structure with respect to the aircraft longitudinal plane $X_B - Z_B$, the structural analysis is limited to the left-side part.

2.1. Geometry and material

In this study, the PrP wing-box architecture is optimised in the framework of the preliminary design phase of the aeronautic industry. During this phase, several loading conditions are considered to properly design the main components of the structure in order to respect certification specifications [42]. Such load cases (LCs) result from the combination of basic loading conditions (BLCs) of different nature, e.g. flight loads due to

symmetrical and asymmetrical manoeuvres or to gusts, ground loads, pressurisation, etc. In this work, only a sub-set of these LCs is considered, as explained in Section 2.3.

For each wing of the PrP configuration, the external geometry is assigned in terms of the leading edge (LE) coordinates of three fundamentals sections, i.e. root, kink and tip, as well as the chord length at each of the three locations. The geometrical features affecting the out-plane shape of the wing, i.e. dihedral and twist angles, are also taken into account. All of the aforementioned quantities, which are summarised in Table 1, are known at the three sections (only two for the VW, which does not present a kink section), and linearly vary between them.

For the sake of simplicity, a polynomial interpolation of the dorsal and ventral edges of the supercritical aerofoil F15 − 11, illustrated in Fig. 3 and taken from [43], is considered. A polynomial of degree five constitutes a good approximation of the actual profile. This profile is used to describe the shape of the wing sections parallel to the free-stream direction. As for the wing-box, its position, in chord percent, is fixed *apriori*. According to

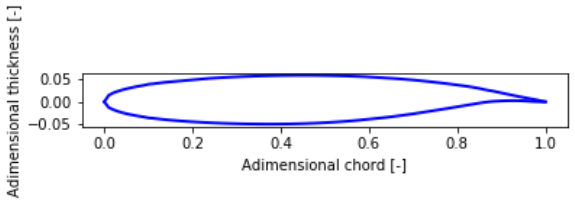

Figure 3: Aerofoil F15-11

[43], a span-wise linear behaviour of both front and rear spars, for each wing, is adopted. The position of spars, with respect to the considered wing planform, is shown in Fig. 4 and reported in Tab. 2.

Regarding the modelling of the structural components, the following simplifications are introduced:

1. only major structural components are modelled (i.e. skin, stringers, ribs and spars);
2. the interfaces between the structural components are perfect (i.e. the perfect bonding condition applies);
3. connection zones and opening/cut-out are neglected and not considered into the preliminary design phase.

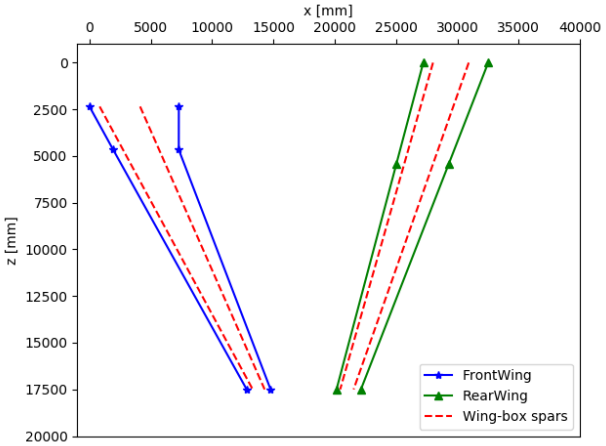

Figure 4: Planform of the PrP lifting system, with wing-box position

Table 1: Wing geometry

	LE coordinates [mm]	Chord [mm]	Twist angle [deg]
Front Wing			
Root	$(0, 0, 2350)$	7287	3.05
Kink	$(1932, 200, 4661)$	5350	3.9
Tip	$(12820, 810, 17500)$	1949	1.5
Rear Wing			
Root	$(26138, 7926, 0)$	5295	3.7
Kink	$(23955, 7926, 5400)$	4276	2.99
Tip	$(19064, 7926, 17500)$	1991	1.4
Vertical Wing			
Root	$(13623, 1310, 18000)$	1852	1.5
Tip	$(18261, 7426, 18000)$	1922	1.4

Table 2: Wing-box position (reported in chord percent, refer to the planform of Fig. 4)

	Root	Kink	Tip
Front Wing	11%	15%	25%
	57%	70%	75%
Rear Wing	15%	15%	15%
	70%	70%	70%
Vertical Wing	20%	-	20%
	80%	-	77%

For both FW and RW, ribs are parallel to the free stream direction between root and kink sections, whilst they are perpendicular, respectively, to the rear and front spar between kink and tip sections (see Figs. 5 and 8). For the VW, ribs are perpendicular to both front and rear spars. However, in order to ensure a gradual change in the orientation between root-kink and kink-tip sectors, some transition ribs at intermediate angles are

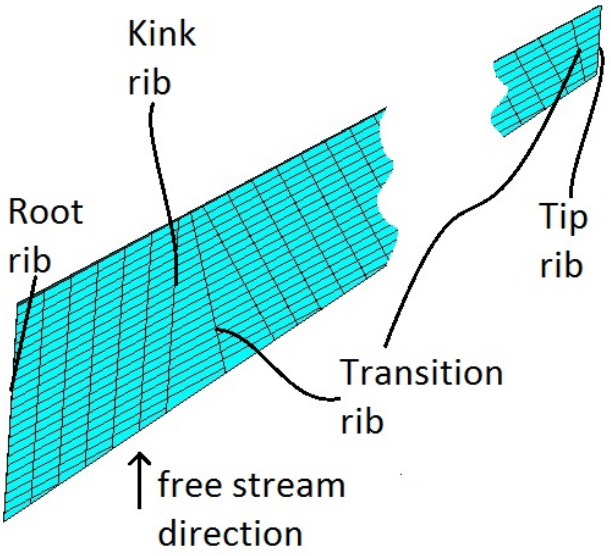

Figure 5: Ribs orientation (detail of the FW architecture)

introduced, as illustrated in Figs. 5 and 8. Inasmuch as the goal of the proposed methodology is the preliminary optimisation of the PrP wing-box architecture, a simplified rib geometry is considered, as shown in Fig. 6, with a constant thickness equal to 4 mm, as often done in the literature [44–46]. Stringers have a T-shaped cross-section, while spar

Figure 6: Rib simplified geometry (FW root section)

caps have a L-shaped cross-section, as illustrated in Fig. 7. Their geometric parameters represent some of the variables of the PrP wing-box least-weight design problem and will be discussed in Section 3.1. It is noteworthy that both GFEM and LFEM, presented in Section 4, do not take into account for explicit modelling of shear tie, stringer-tie and tear-strap. In particular, in the LFEM these features are implicitly modelled by means of suitable interface elements, as discussed in Section 4.2.

The material behaviour for each structural element constituting the PrP wing-box is assumed to be linear elastic homogeneous isotropic. Two alloys have been used: an AA2024-type for shell-like components (i.e. skin, ribs and spar web) and an AA7075-type for stiffener-like components (i.e. stringers and spar caps). The elastic properties for both

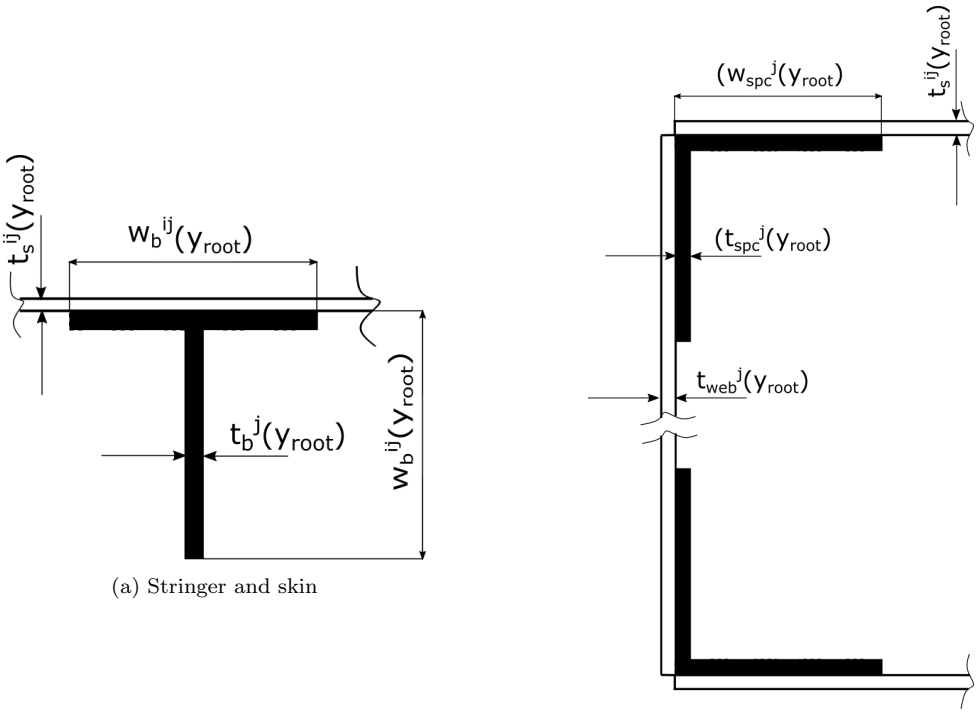

(a) Stringer and skin

(b) Spar and spar caps

Figure 7: Stringer-skin assembly and spar geometry.

alloys are resumed in Tab. 3. Figure 8 gives an overview of the resulting PrP wing-box

Table 3: Material properties

Material	Young's modulus	Poisson's ratio	Density	Yielding stress	Ultimate stress
AA2024	72.4 [GPa]	0.33	2780 [Kgm^{-3}]	290 [MPa]	434 [MPa]
AA7075	71.0 [GPa]	0.33	2810 [Kgm^{-3}]	450 [MPa]	500 [MPa]

geometry.

2.2. Design criteria

Three main families of design criteria can be identified for aeronautic structures, i.e. criteria related to: (a) static loads, (b) fatigue loads and (c) aeroelasticity phenomena.

As far as static loads are concerned, certification specifications [42] identify two types of loading conditions: limit loads (LLs) and ultimate loads (ULs). LLs are the maximum loads expected in service that the structure must be able to support without detrimental permanent deformations. ULs are equal to limit loads multiplied by a prescribed safety factor (usually 1.5). The structure must withstand ULs without failure for at least 3 seconds. For instance, for civil aircraft, LLs in symmetrical manoeuvres occur at load

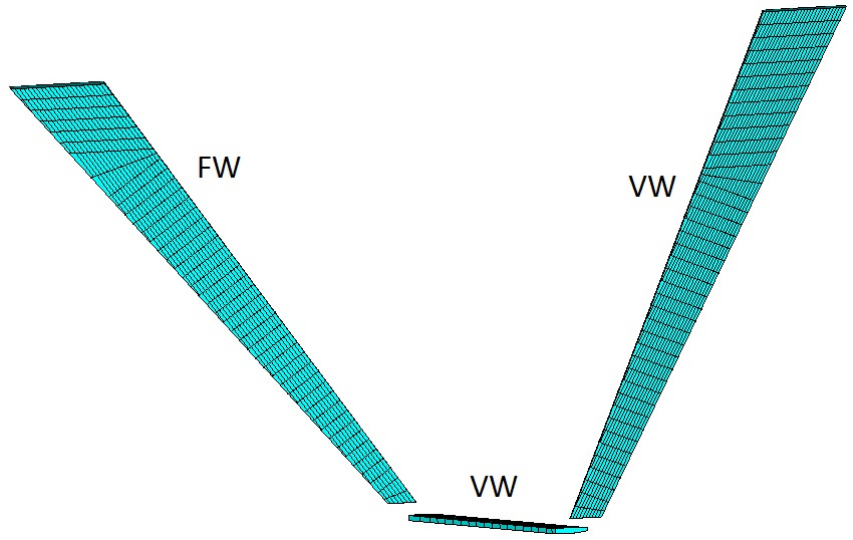

(a) Top view

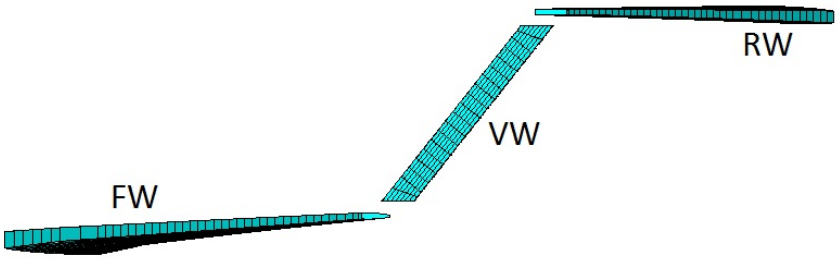

(b) External lateral view

Figure 8: Overview of the PrP wing-box architecture

factors (the ratio of the aerodynamic force component normal to the longitudinal axis of the aeroplane to its weight, measured in the $\mathcal{T}_B$ reference frame, as shown in Fig. 2) $n_z = 2.5$ and $n_z = 1$. This study focuses on this class of design criteria.

Regarding fatigue loads, the design of the structure should be performed in such a way that "catastrophic failure due to fatigue, manufacturing defects, environmental deterioration, or accidental damage, must be avoided throughout the operational life of the aeroplane" [42]. To achieve this goal, two approaches are possible. On the one hand, in the framework of the durability approach, a component should be designed to last the whole operational life. On the other hand, according to the damage tolerance approach, a potential damage in the structure should not become critical before the next planned inspection. In this work, only a fatigue design criterion in the context of the durability approach is employed in terms of an equivalent static check (more details are given in the followings).

Finally, no aeroelastic criteria are considered.

The following set of design criteria (DCs) is integrated in the formulation of the multi-scale optimisation problem.

- DC1: The global stiffness of the structure must be greater than a predefined reference value.
- DC2: The average equivalent stress in skin, stringers and spars, multiplied by a safety factor $F_S = 1.5$ (see CS 25.303 [42]), must not exceed the yielding stress of the material under LLs.
- DC3: The average equivalent stress in skin, stringers and spars should not exceed the ultimate strength of the material when ULs are considered.
- DC4: No buckling must occur in the stiffened panels when ULs are applied (no-buckling design approach).
- DC5: No critical fatigue failure must occur when a suitable Ground-Air-Ground (GAG) load spectrum is applied.
- DC6: Only manufacturable solutions should be considered.

DC1 is expressed in terms of maximum tip displacement of the lifting system in the flight envelope. DC2 and DC3 are expressed in terms of the average equivalent stress in order to neglect the effects of local stress concentrations that could affect the solution, because of the limited degree of accuracy of the FE models used during the preliminary design phase. Indeed, these criteria are rigorously checked (by means of refined 3D FE models) during the subsequent detailed design phase. DC4 is expressed in terms of no-buckling condition for the most critical stiffened panels identified into the lifting system by means of suitable criteria (discussed in Section 4.2). Of course, the evaluation of the first buckling load of each stiffened panel is done through LFEMs (see Section 4.2).

DC5 is expressed by means of the so-called detail fatigue rating (DFR) method [47]:

$$\sigma_{alt} = \frac{0.47\,\mathrm{DFR}\,(\sigma_{m0} - \sigma_{avg})}{\sigma_{m0} - 0.53\,\mathrm{DFR}} S_w^{5-\log N}, \tag{1}$$

where DFR is a parameter depending on the geometry and it corresponds to a fatigue life of 10^5 cycles based on a reliability level of 0.95 for a particular structural component. Under the hypothesis that the recommended DFR of a structural detail is independent of the aircraft class, in this study its value have been set to DFR = 138 MPa. σ_{m0} and S_w are properties depending upon the considered material (σ_{m0} = 310 MPa and $S_w = 2$ for an aluminium alloy [48]), whilst σ_{alt} is the equivalent stress amplitude of the load cycle which causes failure of the structural element at N cycles, σ_{avg} is the average stress of the load cycle. Using a target life of 75000 flights [49], and the load spectrum of a commercial A320 reported in [50], the cumulative damage can be evaluated by the well-known Miner formula [51].

DC6 is expressed in terms of minimum thickness and relative geometrical proportions of components, as discussed in Section 3.1.

2.3. Load cases

Aerodynamic loads are derived from an in-house algorithm, developed at University of Pisa [52, 53]. This algorithm, called AEROSTATE (AERodynamic Optimisation with STAtic stability and Trim Evaluator), is based on the AVL (Athena Lattice Vortex) method [54] as a solver, and it has been used for the preliminary study for the reference configuration definition, together with medium and high fidelity corrections. For more details, the reader is addressed to [41, 55, 56]. The resulting lift distribution is interpolated and decomposed into a set of point forces and moments (applied to the ribs of each wing) to obtain a statically-equivalent system of forces. The aerodynamic loads are evaluated for a Mach number of 0.79, altitude of 11000 m, adopting the Standard Atmosphere model, in cruise condition. These loads define the fundamental BLC used in this study which is denoted as $\mathrm{BLC_{1g}}$. It is noteworthy that the loads resulting from AEROSTATE code are trimmed with respect to an estimate of aircraft weight and center of gravity position, performed in the algorithm (the resulting configuration is stable in the longitudinal plane from flight mechanics point of view)[41, 55, 56].

For the sake of simplicity, five LCs have been considered. The first one (LC1) corresponds to a load factor $n_z = 2.5$ (pull-up manoeuvre), whilst the second one (LC2) is characterised by $n_z = -1$ (push-down manoeuvre), according to the flight envelope for

civil transport aircraft. Furthermore, third (LC3) and fourth (LC4) loading conditions correspond to $n_z = 3.75$ and $n_z = -1.5$, respectively. The lift distribution for all the previous cases is obtained by a simple scaling of the BLC_{1g} which has been calculated for $n_z = 1$. The fifth loading condition (LC5) is devoted to fatigue strength calculation and it is obtained through a suitable scaling of BLC_{1g} by applying the spectrum of load factors taken from [50].

It is noteworthy that the proposed strategy allows the user to provide as many load conditions as needed. Moreover, the five considered LCs are commonly used in the preliminary design of civil aircraft wing-box structures at the boundary of the flight envelope [46, 57].

Table 4 summarises the LCs together with the relative DCs.

Table 4: Load cases definition and associated design criterion

LC	BLC_{1g} factor	DC
1	2.5	1,2,6
2	-1	1,2,6
3	3.75	3,4,6
4	-1.5	3,4,6
5	variable for each cycle, taken from [50]	5

3. Mathematical formulation of the optimisation problem

3.1. Design variables

Only geometrical design variables have been considered in this study. They can be grouped with respect to the component they are referred to. Moreover, these variables are related to the components of each wing, i.e. FW, RW and VW.

Firstly, the design variables related to the components of the VW are not independent and are obtained as the average of their counterparts for both FW and RW. Secondly, for each wing, different design variables are affected to the components located in the dorsal and ventral region of the wing. The description of the geometric design variables is given in the followings, component by component.

Stringers and skin

For each wing, stringers and skin have different size for dorsal and ventral regions. In particular, as shown in Fig. 7, the generic stringer has a T-shaped cross-section and two variables are needed, at each location along the wing span, to fully describe its geometry, i.e.

$$t_{\mathrm{b}}^{j}(y)\,,\ w_{\mathrm{b}}^{ij}(y)\,,\ i=\mathrm{top},\mathrm{bot},\ j=\mathrm{FW},\mathrm{RW}. \tag{2}$$

In the above equation, y is the Cartesian coordinate defined along the wing span, t_{b}^{i} is the thickness, whilst w^{ij} is the flange width. Conversely, the skin needs only one geometric variable, i.e. the thickness, to be characterised:

$$t_{\mathrm{s}}^{ij}(y)\,,\ i=\mathrm{top},\mathrm{bot},\ j=\mathrm{FW},\mathrm{RW}. \tag{3}$$

A further variable, characterising the skin-stringers assembly, is the stringer pitch, which can be different between dorsal and ventral regions, i.e.

$$p^{ij},\ i=\mathrm{top},\mathrm{bot},\ j=\mathrm{FW},\mathrm{RW}. \tag{4}$$

Spars and spars caps

As illustrated in Fig. 7, the spar geometry is relatively simple, and it is composed of a web and two spar caps with a L-shaped cross-section. In particular, the geometric parameters of the spar caps are not independent and are related to those of the stringers as follows:

$$\begin{aligned} w_{\mathrm{spc}}^{j}(y) &= \frac{w^{\mathrm{top}j}(y)+w^{\mathrm{bot}j}(y)}{2},\\ t_{\mathrm{spc}}^{j}(y) &= \frac{t_{\mathrm{b}}^{\mathrm{top}j}(y)+t_{\mathrm{b}}^{\mathrm{bot}j}(y)}{2},\\ j &= \mathrm{FW},\mathrm{RW}, \end{aligned} \tag{5}$$

where $w_{\mathrm{spc}}^{j}(y)$ and $t_{\mathrm{spc}}^{j}(y)$ are the width and the thickness of the spar cap flanges at a given location y along the wing span, for each wing, see Fig. 7. As it can been inferred

from the above relationships, each quantity is evaluated as the average of the respective counterpart of the stringers. Regarding the spar web, its thickness varies along the wingspan as follows:

$$t^j_{\text{web}}(y)\,,\ j = \text{FW}, \text{RW}. \tag{6}$$

Ribs

As discussed in Section 2.1, a simplified rib geometry is considered in this work, as shown in Fig. 6, with a constant thickness equal to 4 mm. Of course, the rib in-plane shape is scaled according to its position and orientation along the wing span. Since the geometric variables of the ribs are kept constant, as usually done in the literature [44–46] during the preliminary design phase, only the pitch between adjacent ribs (for each wing) is included among the design variables, i.e.

$$p^j_{\text{r}},\ j = \text{FW}, \text{RW}. \tag{7}$$

Among the aforementioned design variables, those varying along the wing span abscissa can be expressed as:

$$\begin{aligned} &\xi^{ij}(y) = \xi^{ij}(y_{\text{root}}) + \frac{\xi^{ij}(y_{\text{root}})(\alpha^j - 1)}{y_{\text{tip}} - y_{\text{root}}}(y - y_{\text{root}}), \\ &i = \text{top}, \text{bot},\ j = \text{FW}, \text{RW}, \end{aligned} \tag{8}$$

with

$$\begin{aligned} &\alpha^j = \begin{cases} \alpha^j_{\text{s}},\ \text{if } \xi^{ij}(y) = t^{ij}_{\text{s}}(y),\ t^j_{\text{web}}(y), \\ \alpha^j_{\text{b}}\ \text{if } \xi^{ij}(y) = w^{ij}_{\text{b}}(y),\ t^j_{\text{b}}(y),\ w^j_{\text{spc}}(y),\ t^j_{\text{spc}}(y), \end{cases} \\ &i = \text{top}, \text{bot},\ j = \text{FW}, \text{RW}. \end{aligned} \tag{9}$$

In the above equation, α^j_{s} and α^j_{b} are further design variables defining the linear scaling of the relative geometric variables along the wing span. As it can be easily inferred from Eq. (8), the generic geometric design variable of each component linearly varies along

the wing span. Therefore, the *independent design variables* are the geometric parameters characterising the structural elements at the root section (for each wing) and the scaling parameters. Accordingly, all the independent design variables can be collected into the vector of design variables $\boldsymbol{\xi}$ as follows:

$$\begin{aligned} \boldsymbol{\xi}^{\mathrm{T}} &= \left\{ \alpha_{\mathrm{s}}^{j}, \alpha_{\mathrm{b}}^{j}, t_{\mathrm{s}}^{ij}(y_{\mathrm{root}}), t_{\mathrm{b}}^{j}(y_{\mathrm{root}}), w_{\mathrm{b}}^{ij}(y_{\mathrm{root}}), t_{\mathrm{web}}^{j}(y_{\mathrm{root}}), p_{\mathrm{r}}^{j}, p^{ij} \right\}, \\ & i = \mathrm{top}, \mathrm{bot}, \;\; j = \mathrm{FW}, \mathrm{RW}. \end{aligned} \tag{10}$$

The design variables together with their lower and upper bounds are summarised in Tab. 5 ($i = \mathrm{top}, \mathrm{bot}, \;\; j = \mathrm{FW}, \mathrm{RW}$).

Table 5: Lower and upper bounds of the design variables

Variable	Description	Lower bound	Upper bound	Sampling
α_{s}^{j} [−]	Scaling parameter	0.1	1	0.01
α_{b}^{j} [−]	Scaling parameter	0.1	1	0.01
$t_{\mathrm{s}}^{ij}(y_{\mathrm{root}})$ [mm]	Skin thickness (root)	1.3	15	0.1
$t_{\mathrm{b}}^{j}(y_{\mathrm{root}})$ [mm]	Stringers thickness (root)	1.3	15	0.1
$w_{\mathrm{b}}^{ij}(y_{\mathrm{root}})$ [mm]	Stringers flange length (root)	32	70	1
$t_{\mathrm{web}}^{j}(y_{\mathrm{root}})$ [mm]	Spar web thickness (root)	1.3	15	0.1
p_{r}^{j} [mm]	Ribs pitch	300	600	50
p^{ij} [mm]	Stringers pitch	100	140	10

3.2. Objective and constraint functions

The goal of the MSO strategy is the minimisation of the total mass of the PrP wingbox architecture which represents the objective function $\Phi(\boldsymbol{\xi})$ for the problem at hand, i.e.

$$\Phi(\boldsymbol{\xi}) = 2 \sum_{e=1}^{N_e} V_e(\boldsymbol{\xi}) \rho_e, \tag{11}$$

where $V_e(\boldsymbol{\xi})$ and ρ_e are the volume and the density of the e-th element, whilst N_e is the total number of elements composing the GFEM of the left wing (due to the symmetry

with respect to the aircraft longitudinal plane).

Let Ω be the geometrical domain of the (semi) model of the PrP lifting system. According to Fig. 8, it can be split as: $\Omega = \Omega_{\mathrm{FW}} \cup \Omega_{\mathrm{RW}} \cup \Omega_{\mathrm{VW}}$, where each sub-set is related to the corresponding wing. Furthermore, as stated above, the geometrical variables of the VW depend upon those of both FW and RW, thus they are not included among the design variables. It is noteworthy that the geometric set of each wing can be decomposed as

$$\begin{aligned} &\Omega^j = \Omega_s^{ij} \cup \Omega_{\mathrm{b}}^{ij} \cup \Omega_{\mathrm{web}}^{j} \cup \Omega_{\mathrm{spc}}^{ij} \cup \Omega_r^{j}, \\ &i = \mathrm{top}, \mathrm{bot}, \;\; j = \mathrm{FW}, \mathrm{RW}. \end{aligned} \tag{12}$$

Therefore, the geometric domain of each wing is composed of external skin, stringers, spar webs, spar caps (for both dorsal and ventral regions) and ribs.

Before illustrating the problem formulation, it is useful to introduce two further subsets. $\Omega_{\mathrm{c-GFEM}} \subset \Omega_j$ is a subset of $\Omega_{\mathrm{FW}} \cup \Omega_{\mathrm{RW}}$ belonging to the GFEM which identifies the *checking zone*, i.e. that zone where stresses get meaningful values to be considered within the DCs. Conversely, $\Omega_{\mathrm{c-LFEM}} \subset \Omega_{\mathrm{c-GFEM}}$ is a sub-region of the GFEM checking zone used to build the LFEM representing the most critical stiffened panel (within FW and RW).

Taking into account the previous notation, DC1 is formulated as follows [18]:

$$g_1 := \max_{\mathbf{LC}=\{1,2\}} \frac{|\delta_{\mathrm{tip-FW}}|}{\mathrm{b}} - 0.15 \leq 0, \; \mathrm{in}\, \Omega_{\mathrm{FW}}, \tag{13}$$

where b is the nominal semi-span, $\delta_{\mathrm{tip-FW}}$ is the vertical displacement at the tip, conventionally measured at the FW, under either LC1 or LC2.

DC2 is formulated by imposing that the Von-Mises equivalent stress in skin, stringers and spars, within the checking zone of the GFEM $\Omega_{\mathrm{c-GFEM}}$, must be lower than the yielding stress of the material. For LC1 and LC2, skin must not reach the yielding stress (considering a safety factor of 1.5), i.e.

$$\begin{aligned} &g_2 := \max_{\mathbf{LC}=\{1,2\}} \frac{\sigma_{\mathrm{VM}}}{\sigma_{y\,2024}} - \frac{1}{1.5} \leq 0, \;\; \mathrm{in}\; \Omega_s^{ij} \cap \Omega_{\mathrm{c-GFEM}}, \\ &i = \mathrm{top}, \mathrm{bot}, \;\; j = \mathrm{FW}, \mathrm{RW}. \end{aligned} \tag{14}$$

$$
\begin{aligned}
&g_3 := \max_{\mathbf{LC}=\{1,2\}} \frac{\sigma_{\mathrm{VM}}}{\sigma_{y\,7075}} - \frac{1}{1.5} \leq 0, \;\; \text{in } \Omega_{\mathrm{b}}^{ij} \cap \Omega_{\mathrm{c-GFEM}}, \\
&i = \mathrm{top}, \mathrm{bot}, \;\; j = \mathrm{FW}, \mathrm{RW},
\end{aligned}
\tag{15}
$$

$$
\begin{aligned}
&g_4 := \max_{\mathbf{LC}=\{1,2\}} \frac{\sigma_{\mathrm{VM}}}{\sigma_{y\,7075}} - \frac{1}{1.5} \leq 0, \;\; \text{in } \Omega_{\mathrm{web}}^{j} \cap \Omega_{\mathrm{c-GFEM}}, \\
&j = \mathrm{FW}, \mathrm{RW},
\end{aligned}
\tag{16}
$$

where σ_{VM} is the Von-Mises equivalent stress and σ_{y2024} and σ_{y7075} are the yielding stresses for AA2024 and AA7075, respectively, reported in Tab. 3.

As far as DC3 is concerned, it is formulated by imposing that the Von-Mises equivalent stress must be lower than the ultimate stress of the material for skin, stringers and spars within the checking zone of the GFEM:

$$
\begin{aligned}
&g_5 := \max_{\mathbf{LC}=\{3,4\}} \frac{\sigma_{\mathrm{VM}}}{\sigma_{u\,2024}} - 1 \leq 0, \;\; \text{in } \Omega_{s}^{ij} \cap \Omega_{\mathrm{c-GFEM}}, \\
&i = \mathrm{top}, \mathrm{bot}, \;\; j = \mathrm{FW}, \mathrm{RW}.
\end{aligned}
\tag{17}
$$

$$
\begin{aligned}
&g_6 := \max_{\mathbf{LC}=\{3,4\}} \frac{\sigma_{\mathrm{VM}}}{\sigma_{u\,7075}} - 1 \leq 0, \;\; \text{in } \Omega_{\mathrm{b}}^{ij} \cap \Omega_{\mathrm{c-GFEM}}, \\
&i = \mathrm{top}, \mathrm{bot}, \;\; j = \mathrm{FW}, \mathrm{RW},
\end{aligned}
\tag{18}
$$

$$
\begin{aligned}
&g_7 := \max_{\mathbf{LC}=\{3,4\}} \frac{\sigma_{\mathrm{VM}}}{\sigma_{u\,7075}} - 1 \leq 0, \;\; \text{in } \Omega_{\mathrm{web}}^{j} \cap \Omega_{\mathrm{c-GFEM}}, \\
&j = \mathrm{FW}, \mathrm{RW},
\end{aligned}
\tag{19}
$$

where σ_{u2024} and σ_{u7075} are the ultimate stresses for AA2024 and AA7075, respectively, as reported in Tab. 3.

Regarding DC4, it involves an eigenvalue buckling analysis performed on the most critical stiffened panel extracted from the checking zone belonging to the GFEM, i.e. it is

checked on $\Omega_{\text{c-LFEM}}$. It is expressed through the following inequality:

$$g_8 := \max_{\mathbf{LC}=\{3,4\}} \left(1 - \frac{\lambda}{1.05}\right) \leq 0, \text{ in } \Omega_{\text{c-LFEM}}, \tag{20}$$

where λ is the first buckling factor resulting from the LFEM.

DC5 is formulated as follows:

$$g_9 := 7.5 \sum_{i=1}^{p} \frac{n_i}{N_i} - \frac{1}{4} \leq 0, \tag{21}$$

where n_i are the occurrences of the i-th out of p type of cyclic loads (defined as variations of n_z and characterised by average and amplitude stresses), whilst N_i is the number of cycles to get failure evaluated by means of Eq. (1). Since the target life is 75000 flights [49], and since the load spectrum in [50] contains 10066 flights, a correction factor equal to 7.5 has been added.

Finally, DC6 is expressed by means of a set of explicit inequalities on the design variables. Let $t_{\min} = 1.3$ mm be the minimum admissible thickness; the skin thickness at the tip section must be greater than or equal to $t_{\min}$:

$$g_{10-13} := 1 - \frac{t_{\text{s}}^{ij}(y_{\text{root}})\alpha_{\text{s}}^{j}}{t_{\min}} \leq 0, \ i = \text{top}, \text{bot}, \ j = \text{FW}, \text{RW}. \tag{22}$$

Similar relationships apply for stringers and spar webs thickness at the tip section:

$$g_{14-15} := 1 - \frac{t_{\text{b}}^{j}(y_{\text{root}})\alpha_{\text{b}}^{j}}{t_{\min}} \leq 0, \ j = \text{FW}, \text{RW}, \tag{23}$$

$$g_{16-17} := 1 - \frac{t_{\text{web}}^{j}(y_{\text{root}})\alpha_{\text{s}}^{j}}{t_{\min}} \leq 0, \ j = \text{FW}, \text{RW}. \tag{24}$$

The ratio of the stringer flange width (at the root section) to the stringer pitch must be lower than 0.5, i.e.

$$g_{18-21} := \frac{w_{\text{b}}^{ij}(y_{\text{root}})}{p^{ij}} - 0.5 \leq 0, \ i = \text{top}, \text{bot}, \ j = \text{FW}, \text{RW}. \tag{25}$$

The minimum width of the stringer flanges (at the tip section for both wings) must be greater than or equal to $w_{\min} = 32$ mm (this constraint is related to rivet joints).

$$g_{22-25} := 1 - \frac{w_{\mathrm{b}}^{ij}(y_{\mathrm{root}})\alpha_{\mathrm{b}}^{j}}{w_{\min}} \leq 0, \;\; i = \mathrm{top}, \mathrm{bot}, \;\; j = \mathrm{FW}, \mathrm{RW}. \tag{26}$$

Finally, stringers thickness must not be too much different from the skin thickness:

$$g_{26-29} := 0.8 - \frac{t_{\mathrm{b}}^{j}(y_{\mathrm{root}})\alpha_{\mathrm{b}}^{j}}{t_{\mathrm{s}}^{ij}(y_{\mathrm{root}})\alpha_{\mathrm{s}}^{j}} \leq 0, \;\; i = \mathrm{top}, \mathrm{bot}, \;\; j = \mathrm{FW}, \mathrm{RW}. \tag{27}$$

Formally, the least-weight design problem of the PrP lifting system can be stated as a classical CNLPP as follows:

$$\begin{aligned} \underset{\boldsymbol{\xi}}{\text{minimize}} \quad & \Phi(\boldsymbol{\xi}), \\ \text{subject to} \quad & g_i(\boldsymbol{\xi}, \boldsymbol{LC}) \leq 0, \;\; i = 1, \ldots, 29, \\ & \mathbf{lb} \leq \boldsymbol{\xi} \leq \mathbf{ub}, \end{aligned} \tag{28}$$

where **lb** and **ub** are, respectively, the lower and upper bound vectors (see Table 5).

3.3. Numerical strategy

Problem (28) is a non-convex CNLPP. The total number of design variables is 22, whilst the number of optimisation constraints is 29. For the resolution of problem (28) the GA ERASMUS [28] coupled with both GFEM and LFEMs of the structure has been utilised as optimisation tool to perform the solution search, according to the flowchart illustrated in Fig. 9. The GA ERASMUS has already been successfully applied to solve different kinds of engineering problems, see for example [29, 31–37, 58, 59].

For each individual, at each iteration, the numerical tool performs global and local FE analyses to calculate the objective function and the optimisation constraints. In particular, ERASMUS generates an input file (INPUT_ANSYS.TXT) containing the current values of the design variables, i.e. the components of $\boldsymbol{\xi}$. Then, ERASMUS invokes the macro ANSYS.MAC, i.e. the main macro implemented in ANSYS® Parametric Design Language (APDL), which creates both GFEM and LFEMs. This macro invokes the executable file PYTHONEVAL.EXE, which is responsible for the wings geometry description.

In particular, the executable file contains several Python scripts which, starting from $\boldsymbol{\xi}$ and the external frozen geometry of the wing, are able to find the 3D-coordinates of the intersection points between skins and stiffeners. Moreover, the executable decomposes the lift distribution into as many forces and moments as many are the ribs, for each of the three wings. Finally, PYTHONEVAL.EXE returns to ANSYS.MAC the updated values of variables p_t^j, p^{ij}: nominal pitch values are modified to ensure equidistant and homogeneously-distributed ribs and stringers.

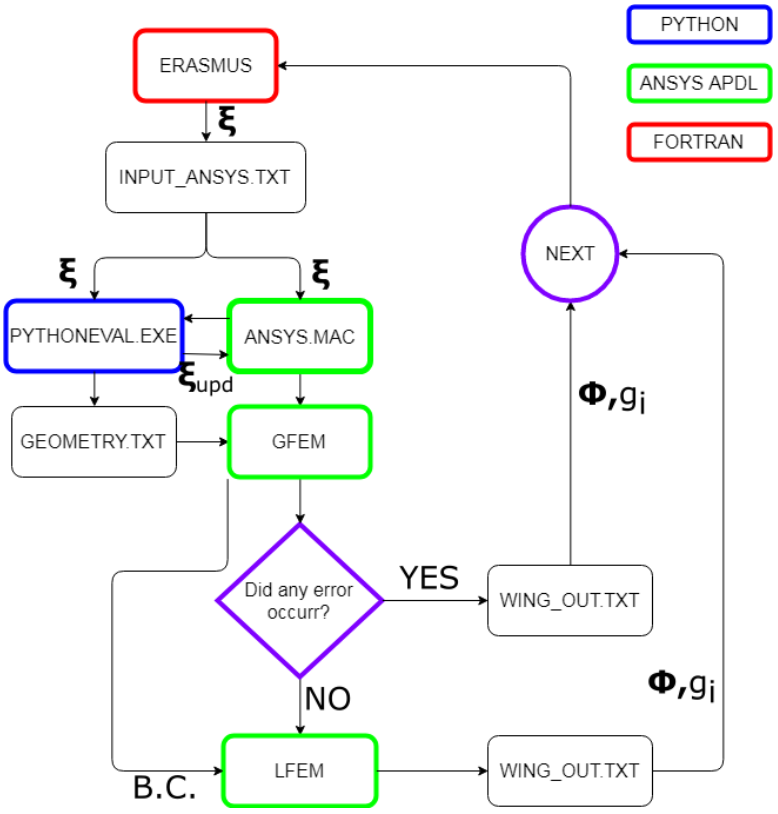

Figure 9: Numerical strategy

If no error occurs in the generation of the GFEM, as detailed in Section 4, for each individual, at each generation, the APDL script performs global and local FE analyses to calculate the objective function and the optimisation constraints. These quantities are passed to the ERASMUS code through the WING_OUT.TXT file.

If an error during the generation of the GFEM occurs (mostly related to the fail of Boolean operations), the objective function and the constraint functions g_i, $i = 1, \ldots, 9$ cannot be computed (because the GFEM and LFEMs cannot be generated). In such a case, they are opportunely penalised and passed to the output file WING_OUT.TXT. All

the details about the modelling strategy are given in Section 4.1.

The GA elaborates the results provided by the GFEM and the LFEMs in order to execute the genetic operations and generate new individuals. These operations are repeated until the GA meets the user-defined convergence criterion.

The generic individual of the GA ERASMUS represents a potential solution for the problem at hand. The genotype of the individual for problem (28) is characterised by only one chromosome composed of 22 genes, each one coding a component of the vector of design variables $\boldsymbol{\xi}$.

4. The global-local finite element modelling approach

As stated above, the FE models integrated in the optimisation process are based on a GL modelling approach. In particular, two different models are created. The GFEM is used to assess the macroscopic behaviour of each wing, whilst refined LFEMs are generated to properly evaluate local responses of the most critical stiffened panels for each region of both FW and RW.

Of course, LFEMs are created only at the critical ZOIs identified during the global analysis, thus suitable criteria must be developed to accomplish this task. Both GFEM and LFEMs are fully parametric and are built using the commercial FE code ANSYS®.

4.1. The global finite element model

As stated in the previous Section, the geometry of each wing is generated by means of the executable PYTHONEVAL.EXE. In particular, the executable returns a file containing the coordinates of the points at the intersection between skins and stiffeners. These information are passed to the APDL script which builds the GFEM. An overview of the GFEM is given in Fig. 8.

Skin, ribs and spar webs are modelled with 4-node SHELL181 elements (Reissner-Mindlin kinematics), while stringers and spar caps are modelled with 2-node BEAM188 elements (Timoshenko's beam model). Beam and shell elements are connected together by node merging. To take into account for the actual position of the beam cross-section with respect to the skin, a section offset is applied to beam elements. Shear-tie components are

not modelled, but their mechanical effect (the transfer of shear load from ribs to skin) is ensured by the direct connection between ribs and skin elements.

When generating the mesh of the whole wing-box, a correction must me introduced, due to the stringers runout. In the GFEM, stringer runouts occur at ribs, as illustrated in Fig. 10. Therefore, as shown in Fig. 11, there would be many 5-Lines clusters which ANSYS® is not able to fill-in with an Area, unless lines lie in the same plane. To

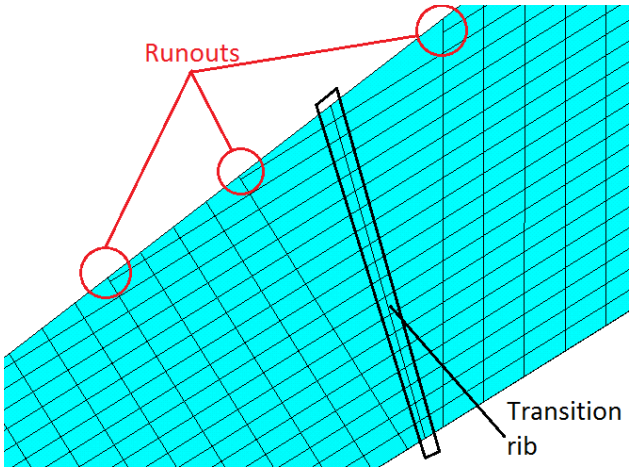

Figure 10: FW kink (particular) and stringers runout.

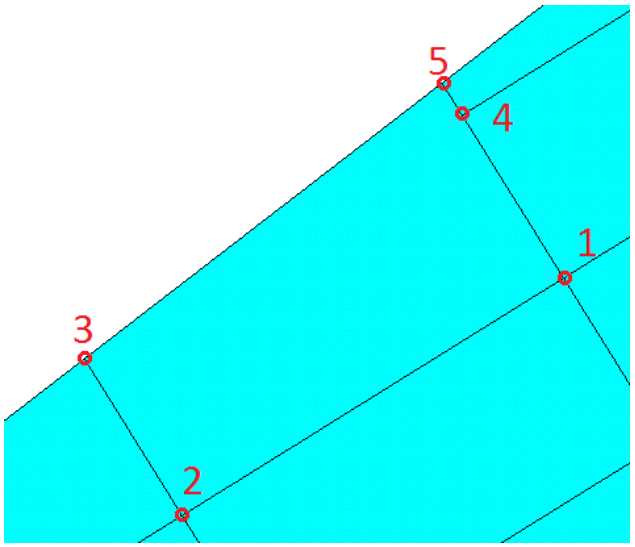

Figure 11: Runout 5-point face

overcome such an issue, the following correction is introduced. With reference to Fig. 11, a plane passing through points 1, 2 and 3 is generated, and points 4 and 5 are forced to lie in such a plane, by modifying their vertical coordinate. Of course, such an operation does not modify significantly the geometry of the wing-box because the magnitude of the

correction is of the order of tenths of millimetre.

The generation of the wing geometry through a dedicated Python routine, as discussed in Section 3.3, is mainly due to the possibility of performing such a correction. Another reason to generate the geometry externally from ANSYS® is is related to the fail of Boolean operations, which may occur for particular configurations. One can create the net representing the intersection of skin with ribs and stringers through intersection of the skin (Area component) with working planes (or other similar methods available in ANSYS®). However, this strategy reveals, often, unstable: the intersections may not be created, depending on the internal tolerance values related to Boolean operations. As a consequence, the geometry is not correctly generated, and this jeopardises the overall optimisation run.

The element type (linear or quadratic) and the mesh size have been chosen after performing a sensitivity analysis, not reported here for the sake of brevity. An automatic check has been implemented to prevent the generation of highly distorted shell elements with a threshold aspect ratio equal to three. The mesh of shell elements is composed mainly of quadrangular elements. Of course, triangular elements may occur in the 5-node areas where stringer runouts take place.

As shown in Fig. 8, fillets connecting FW and RW to VW are not explicitly modelled; MPC184 (multi-point constraint) elements with "rigid beam" behaviour (master-slave approach) are used to link extremal ribs nodes with the central master node, as illustrated in Fig. 12.

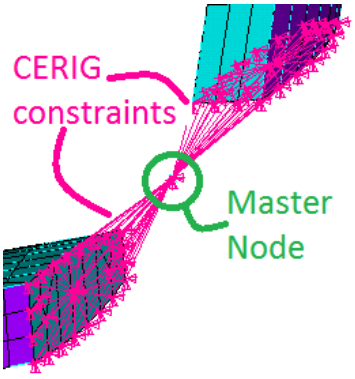

Figure 12: Connection between FW and VW

Aerodynamic forces and moments are applied to a reference node which, for the sake

of simplicity, is created at the centroid of each rib; the master node is then linked to the boundary nodes of each rib via RBE3 elements, as shown in Fig. 13. Since AEROSTATE-

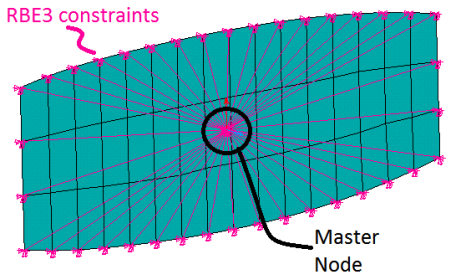

Figure 13: Force and moment application to ribs

AVL gives as an output the position of the pressure center, for each of the strips in which the lifting surface is subdivided, transport moments can be easily evaluated.

As far as BCs of the GFEM are concerned, the 6 DOFs of the nodes lying at the root rib of both FW and RW are null. A typical frontal deformed shape of the PrP wing, for the two considered vertical load factors, is qualitatively illustrated in Fig. 14. It can be appreciated the tendency to invert curvature (invert sign of bending stresses) in proximity of tips [3].

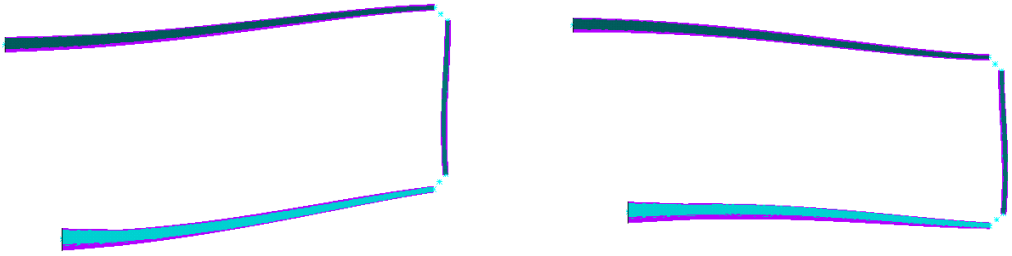

(a) $n_z = 2.5$ (b) $n_z = -1$

Figure 14: Deformed shapes (frontal view)

After solving the GFEM for each LC, the checking zone, i.e. the $\Omega_{\text{c-GFEM}}$ set, is created. When creating $\Omega_{\text{c-GFEM}}$, two bays close to the root section, two bays close to the connection to the VW, and two bays surrounding the kink rib are disregarded. Furthermore, the two closest areas to the front and rear spar caps are not included for each bay; similarly, bays having less then five stringers are not considered. As an example, Fig. 15 shows the checking zone for the dorsal skin of the FW. Of course, the checking zone for stringers and spar webs is generated in a similar way. The union of all these checking

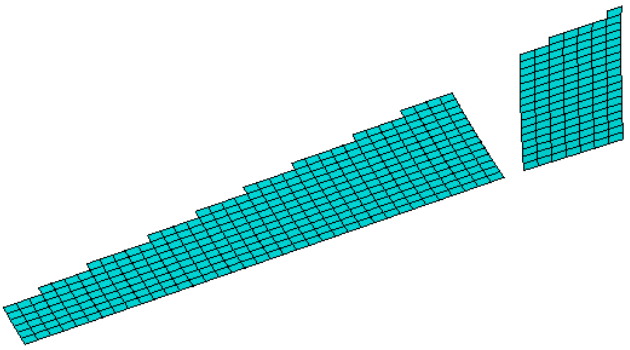

Figure 15: Reading set for FW dorsal skin

zones constitutes the set $\Omega_{\mathrm{c-GFEM}}$.

Results provided by the GFEM are used for the evaluation of the objective function and all the constraint functions except that related to buckling requirement, i.e. g_8 of Eq. (20).

4.2. The local finite element model

LFEMs are generated in order to evaluate structural phenomena which typically appear at a smaller scale with respect to the GFEM one. In this work, the LFEMs are used to assess the first buckling load of the most critical stiffened panel $\Omega_{\mathrm{c-LFEM}}$, as discussed in Section 3.

The automatic generation of LFEMs is anything but trivial, and it is characterised by two issues which can be described through the following questions:

- How can one automatically identify the most critical stiffened panels, i.e. the ZOIs, within the check zone of the GFEM?
- How can one automatically generate a refined FE model (i.e. the LFEM) integrating the neighbourhood of the ZOI and able to describe both primary and secondary buckling modes? In particular, this algorithm must be position-agnostic: the ZOIs can be situated anywhere in $\Omega_{\mathrm{c-GFEM}}$.

Instead of creating a LFEM for each ZOI of each wing, for every LC, in this study only one LFEM is created for the most critical ZOI and for the most critical LC. The user can define *apriori* the number of stringers to be included in the LFEM. For this study, this number has been set equal to five, as shown in Fig. 16. The LFEM considers the portion

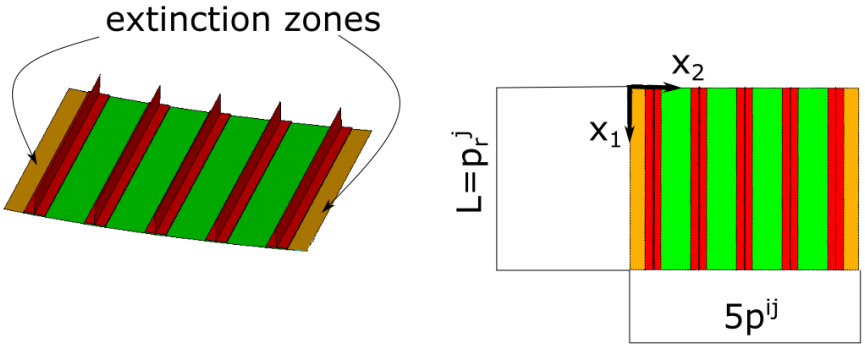

Figure 16: Typical LFEM with 5 stringers (view and dimensions)

of $\Omega_{\mathrm{s}}^{ij} \cup \Omega_{\mathrm{b}}^{ij}$ enclosed by two subsequent ribs; extinction zones of length $\frac{p^{ij}}{2}$ are considered on each side of the stiffened panel to mitigate edge effects due to the application of BCs. The structural components are entirely modelled by using SHELL181 (Reissner-Mindlin kinematics) elements. A dedicated meshing algorithm ensures the presence of at least eight elements in the portion of skin among two consecutive stringers, and element ratio is set as closest to the unitary value as possible.

Stringer flanges are tied to the skin via constraint equations at their interface nodes. MPC184 are used to this purpose, as shown in Fig. 17. Dirichlet-type BCs are interpolated

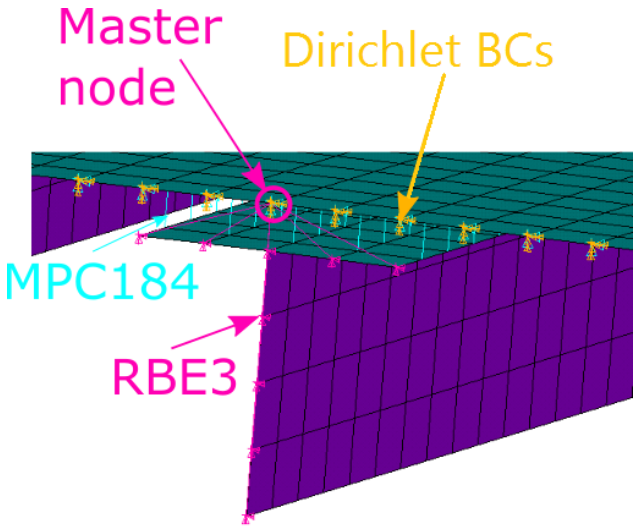

Figure 17: LFEM particular

from the GFEM, for the most critic LC, and applied to the nodes of the skin located at $x = 0$ and $x = L$ (according to the frame of Fig. 16), as illustrated in Fig. 17. The load

transfer from skin edges (where BCs are applied) to stringer edges (located at the same value of the x coordinate) makes use of RBE3 elements, assuming as master the overlying node of the skin, as clearly shown in Fig. 17.

Linear buckling analysis is performed on the LFEM, and the resulting first positive eigenvalue $\lambda(\xi)$ is used for the evaluation of constraint g_8 of Eq. (20).

4.3. Criteria to identify the zones of interest

To keep computational times as low as possible, specific criteria have been implemented in the presented MSO strategy, in order to reduce the number of LFEMs. As stated beforehand, only one LFEM is created, for the most critical area in $\Omega_{\mathrm{c-GFEM}}$, for the most critical LC.

To automatically identify the ZOI, an approximated buckling factor is evaluated for each skin panel delimited by two consecutive ribs and two consecutive stringers. The approximation is based on an analytical formula for simply-supported rectangular plates (having, in the considered case, dimensions p_{r}^{j} and p^{ij}), undergoing constant membrane loads per unit width N_{11}^{s} and N_{22}^{s} (positive if tensile), where axis x_1 is stringer-wise, whilst axis x_2 is normal to x_1 and to the panel medium-plane outward normal. In order to consider the presence of stringers, the normal force per unit length along x_1 axis is evaluated as:

$$N_{11} := N_{11}^{\mathrm{s}} + \frac{P_{\mathrm{b}}^{11}}{p^{ij}}, \tag{29}$$

where P_{b}^{11} is the resultant (averaged) force of the two stringers delimiting the generic plate.

The approximation of the buckling factor, for isotropic material, reads (see [60–62] for the mathematical derivation):

$$\lambda := \min_{m,n} \left(\pi^2 \, D \, \frac{\left(\frac{m}{p_{\mathrm{r}}^{j}}\right)^4 + \left(\frac{n}{p^{ij}}\right)^4 + 6 \left(\frac{m\,n}{p^{ij}\,p_{\mathrm{r}}^{j}}\right)^2}{-N_{11}\left(\frac{n}{p^{ij}}\right)^2 - N_{22}\left(\frac{m}{p_{\mathrm{r}}^{j}}\right)^2} \right), \tag{30}$$

where D is the bending stiffness of the plate having thickness equal to $t_{\mathrm{s}}^{ij} + \frac{A_{\mathrm{b}}^{ij}}{p^{ij}}$, Young's modulus and Poisson's ratio equal to the average of those reported in Tab. 3. A_{b}^{ij} is the

averaged cross-section area of stringers delimiting the plate. Eq. (30) is meaningful only for plates where N_{11} and/or N_{22} are negative (compressive).

Finally, the most critical plate is identified by the Area ID number where $\min_{\text{LCs}}(\lambda)$, with $\lambda \geq 0$ occurs (i.e. the minimum value of λ for each skin panel among all the considered LCs). A dedicated algorithm generates the neighbourhood of such an area: the result is the LFEM, as shown in Fig. 16.

5. Results

The parameters of the GA ERASMUS, used to solve problem (28), are listed in Tab. 6; selection is performed by the roulette-wheel operator. Optimisation constraints are handled via Automatic Dynamic Penalisation (ADP) method [63]. The whole optimisation process requires a computational time of approximately 11 days when four cores of a machine with an Intel Xeon E5-2697v2 processor (2.7-3.5 GHz) are dedicated to the ANSYS® solver.

Table 6: GA ERASMUS parameters

Parameter	Description	Value
n_{pop}	N. of populations	1
n_{ind}	N. of individuals	220
$n_{\text{gen}}^{\text{max}}$	Max. n. of generations	100
p_{cross}	Crossover probability	0.85
p_{mut}	Mutation probability	$1/n_{\text{ind}}$

The history of the best solution, for each generation, is reported in Fig. 18. As it can been inferred from this figure, the best individual (and, thus, all the individuals within the two populations) is infeasible because at least one constraint is not satisfied. However, thanks to the ADP method, the GA is able to find a feasible solution after only 4 iterations and to converge towards a pseudo-optimal solution after 80 generations. The objective function value does not substantially decrease after 80 iterations. The values of design variables for the optimised wing-box configuration are reported in Tab. 7, whilst objective function and most significant constraints values are resumed in Tab. 8.

As shown in Tab. 7, with respect to Tab. 5, some variables lie on the upper bound of the corresponding range; in particular, the rib pitches assume the largest possible values. Furthermore, the optimised solution is characterised by a value of parameter $\alpha_{\text{s}}^{\text{j}}$ near to

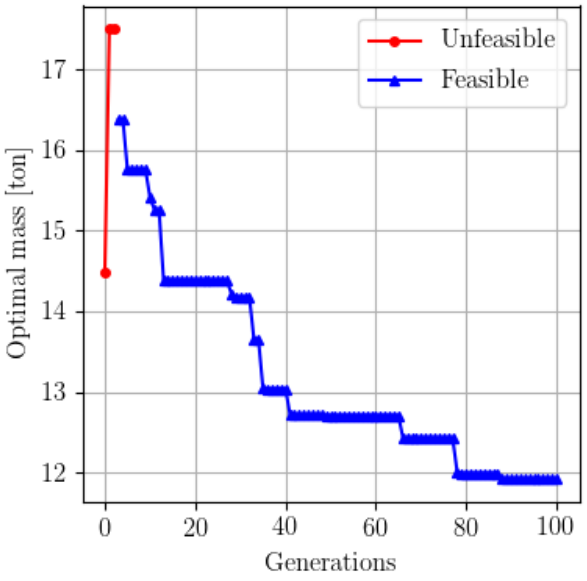

Figure 18: Convergence history

Table 7: Optimisation variables values for the optimal individual

Variable	FW		RW	
	top	bot	top	bot
α_{s}^{j} [−]	0.12		0.21	
α_{b}^{j} [−]	0.66		0.72	
$t_{\mathrm{s}}^{ij}(y_{\mathrm{root}})$ [mm]	13.1	12.4	11.1	7.9
$t_{\mathrm{b}}^{j}(y_{\mathrm{root}})$ [mm]	6.5		9.2	
$w_{\mathrm{b}}^{ij}(y_{\mathrm{root}})$ [mm]	59	68	45	50
$t_{\mathrm{web}}^{j}(y_{\mathrm{root}})$ [mm]	10.9		14.4	
p_{r}^{j} [mm]	600		600	
p^{ij} [mm]	155	155	170	160

Table 8: Objective function and constraints values for the optimal individual

Function	Value
Φ Kg	11920
g_1	−0.303
g_2	−0.001
g_3	−0.247
g_4	−0.034
g_5	−0.331
g_6	−0.359
g_7	−0.452
g_8	−0.291
g_9	−0.057

the lower bound, which means that quantities which scale span-wise with these parameters tend to be as tapered as possible.

It is noteworthy that stringers geometrical dimensions and pitches are almost similar between dorsal and ventral side of both FW and RW. This fact can be justified as follows: for a PrP lifting system, there exist changes in bending curvature in proximity of the wing tips, as shown in Fig. 14. For a given LC, it means that there is no more a single side withstanding tension loads, whilst the other subjected to compression ones, as in conventional wings. This fact implies that both dorsal and ventral regions of each wing must be checked for buckling and static failures, and that both compressive and tension loading conditions are of paramount importance for each region of the structure. The choice of a non-rigid link between FW-VW and RW-VW may alleviate this tendency.

As far as constraints and the final wing-box mass are concerned, Tab. 8 shows that the solution lies on the boundary of static requirements g_2, g_4 and g_9. Buckling is not an active constraint in the optimal solution. This can be explained with the aforementioned fact that the change of curvature in the deformed wing does not give rise to a dramatic compressed zone in proximity of root sections, as expected for conventional wings.

Although a different PrP geometry, in [3] authors obtain a structural mass of 22034 Kg for a MTOW of 230000 Kg (9.58 % of MTOW), for a formulation of problem (28) similar (though simpler) to the one considered in this paper. It must be stressed that the optimised solution obtained in the present study has been searched by means of a more rigorous multi-scale approach, if compared to the problem formulation in [3]. Furthermore, considering additional mass due to systems and other non-structural components, the mass of the complete lifting system, in percentage of MTOW, is close to that of a conventional aircraft. Hence, one may conclude the optimised configuration presented in this paper is likely to be aligned to this trend.

6. Conclusions

A multi-scale optimisation strategy for designing the PrandtlPlane lifting system architecture, by integrating a dedicated global-local modelling approach, has been presented in this work.

The problem has been formulated as a CNLPP, involving constraints of different nature. The formulation of the numerous design requirements needs the assessment of the structure response, at each pertinent scale, under various load cases. To this purpose, fully-parametric scripts have been developed to build global and local FE models in a commercial FE software. The LFEM is automatically generated only for the most critical ZOI, which is identified by means of a suitable criterion, during the GFEM post-processing phase. The solution search has been performed via the GA ERASMUS developed at the I2M laboratory in Bordeaux.

Both the problem formulation and the MSO strategy avoid the introduction of simplifying hypotheses, which may dramatically affect the design space, so preventing the possibility to find a true global optimum solution. Moreover, by employing a global-local FE modelling approach, more accurate and trustworthy results are obtained, with respect to those found by means of simplified models. Finally, the whole process is fully-automated and does not need the user intervention.

The effectiveness of the proposed MSO strategy is proven on a meaningful design case: the structural optimisation of a metallic wing-box of a PrP aircraft. However, the strategy can be easily extended to conventional wing-boxes. The optimised configuration for the presented design case seems to be realistic: results are in agreement with the up-to-date knowledge of PrP aircraft.

As far as perspectives of this work are concerned, the formulation of the problem will be enhanced by taking into account the compliance of the fuselage, for a more realistic design. A preliminary research action is conducted in this sense and aims at developing suitable (i.e. optimised) superelements integrating the fuselage stiffness. In this case, a two-way MSO approach should be realised on both wing and fuselage of the PrandtlPlane in order to obtain a true optimal configuration.

Moreover, research is ongoing in order to extend the MSO strategy to the case of structures made of composite materials, in particular considering blending constraints. Of course, in this case, the design problem formulation must integrate requirements pertinent to composite solutions, e.g. suitable failure criteria at each scale (lamina-level and constitutive phases-level), delamination criteria, manufacturing requirements, etc.

Aknowledgement

This paper presents part of the activities carried out within the research project PARSIFAL (PrandtlPlane ARchitecture for the Sustainable Improvement of Future AirpLanes), which has been funded by the European Union under the Horizon 2020 Research and Innovation Program (Grant Agreement n.723149).

References

[1] L. Prandtl, Induced drag of multiplanes, technical note 182, NACA (1924).

[2] A. Frediani, G. Montanari, Best wing system: An exact solution of the prandtl's problem, in: G. Buttazzo, A. Frediani (Eds.), Variational Analysis and Aerospace Engineering., Vol. 33 of Springer Optimization and Its Applications, Springer, New York, NY, 2009. doi:https://doi.org/10.1007/978-0-387-95857-6_11.

[3] D. Dal Canto, A. Frediani, G. L. Ghiringhelli, M. Terraneo, The lifting system of a prandtlplane, part 1: Design and analysis of a light alloy structural solution, in: G. Buttazzo, A. Frediani (Eds.), Variational analysis and aerospace engineering: mathematical challenges for aerospace design, Vol. 66 of Springer Optimization and Its Applications, Springer, Boston, MA, 2012. doi:https://doi.org/10.1007/978-1-4614-2435-2_9.

[4] N. Divoux, A. Frediani, The lifting system of a prandtlplane, part 2: preliminary study on flutter characteristics, in: G. Buttazzo, A. Frediani (Eds.), Variational Analysis and Aerospace Engineering: Mathematical Challenges for Aerospace Design, Vol. 66 of Springer Optimization and Its Applications, Springer, Boston, MA, 2012. doi:https://doi.org/10.1007/978-1-4614-2435-2_10.

[5] A. Frediani, F. Quattrone, F. Contini, The lifting system of a prandtlplane, part 3: Structures made in composites, in: G. Buttazzo, A. Frediani (Eds.), Variational Analysis and Aerospace Engineering: Mathematical Challenges for Aerospace Design, Vol. 66 of Springer Optimization and Its Applications, Springer, Boston, MA, 2012. doi:https://doi.org/10.1007/978-1-4614-2435-2_11.

[6] L. M. F. Diolosà, Preliminary studies for the structural optimization of a prandtlplane wing, Master's thesis, University of Pisa, Department of Civil and Industrial Engineering, Aerospace division (2018).
URL https://etd.adm.unipi.it/theses/available/etd-09032018-165921/

[7] A. Nardone, Progetto di ali di velivoli leggeri costruite per saldatura di lamiere sottili di alluminio, Master's thesis, University of Pisa, Department of Civil and Industrial Engineering, Aerospace division, in italian (2016).
URL https://etd.adm.unipi.it/theses/available/etd-05222016-162117/

[8] V. Cipolla, V. Binante, A. Nardone, Design, optimization and manufacturing of metallic wings of light aircraft, Aerotecnica Missili e spazio 97 (4) (2018) 219–227. doi:10.19249/ams.v97i4.350.

[9] R. Cavallaro, Nonlinear aeroelastic analysis of joined-wing configurations, Ph.D. thesis, San Diego State University (2014).
URL https://escholarship.org/content/qt1p85h6q2/qt1p85h6q2.pdf

[10] R. Bombardieri, R. Cavallaro, R. Castellanos, F. Auricchio, Studies on lateral-directional coupled flight dynamics and aeroelasticity of a prandtlplane, in: AIAA Scitech 2019 Forum, 2019.
URL https://doi.org/10.2514/6.2019-1118

[11] R. Cavallaro, R. Bombardieri, J. Santos, Discrete gust response of a box-wing configuration, in: 6th CEAS Conference, Bucarest, 2017.

[12] R. Cavallaro, R. Bombardieri, L. Demasi, A. Iannelli, Prandtlplane joined wing: Body freedom flutter, limit cycle oscillation and freeplay studies, Journal of Fluids and Structures 59 (2015) 57–84. doi:10.1016/j.jfluidstructs.2015.08.016.

[13] R. Cavallaro, R. Bombardieri, S. Silvani, L. Demasi, G. Bernardini, Aeroelasticity of the prandtlplane: Body freedom flutter, freeplay, and limit cycle oscillation, in: G. Buttazzo, A. Frediani (Eds.), Variational analysis and aerospace engineering: mathematical challenges for the aerospace of the future, Vol. 116 of

Springer Optimization and Its Applications, Springer, New York, NY, 2016. doi:10.1007/978-3-319-45680-5_3.

[14] O. Dababneha, T. Kipouros, A review of aircraft wing mass estimation methods, Aerospace Science and Technology 72 (2018) 256–266.
URL https://doi.org/10.1016/j.ast.2017.11.006

[15] A. Viglietti, E. Zappino, E. Carrera, Free vibration analysis of variable angle-tow composite wing structures, Aerospace Science and Technology 92 (2019) 114 – 125.
URL http://www.sciencedirect.com/science/article/pii/S1270963819304730

[16] A. Benaouali, S. Kachel, Multidisciplinary design optimization of aircraft wing using commercial software integration, Aerospace Science and Technology 92 (2019) 766 – 776.
URL http://www.sciencedirect.com/science/article/pii/S1270963818324131

[17] A. Zhao, H. Zou, H. Jin, D. Wen, Structural design and verification of an innovative whole adaptive variable camber wing, Aerospace Science and Technology 89 (2019) 11 – 18.
URL http://www.sciencedirect.com/science/article/pii/S1270963818329043

[18] O. Dababneha, T. Kipouros, Influence of high fidelity structural models on the predicted mass of aircraft wing using design optimization, Aerospace Science and Technology 79 (2018) 164–173.
URL https://doi.org/10.1016/j.ast.2018.05.043

[19] A. Arrieta, A. G. Stritz, Optimal design of aircraft structures with damage tolerance requirements, Struct Multidisc Optim. 30 (2005) 155–163. doi:10.1007/s00158-004-0510-0.

[20] P. Ciampa, B. Nagel, M. Tooren, Global local structural optimization of transportation aircraft wings, in: 51st AIAA/ASME/ASCE/AHS/ASC Structures, Struc-

tural Dynamics, and Materials Conference, 2010. doi:https://doi.org/10.2514/6.2010-3098.

[21] V. Chedrik, Two-level design optimization of aircraft structures under stress, buckling and aeroelasticity constraints, in: 10th World Congress on Structural and Multidisciplinary Optimisation, 2013.

[22] V. Chedrik, S. Tuktarov, Structural design of aircraft wing based on topology and global-local optimization, in: 11th World Congress on Structural and Multidisciplinary Optimisation, 2015.
URL http://web.aeromech.usyd.edu.au/WCSMO2015/papers/1160_paper.pdf

[23] Q. Liu, J. Mohamed, B. M. Sameer, K. K. Rakesh, Integrated global wing and local panel optimization of aircraft wing, in: 56th AIAA/ASCE/AHS/ASC Structures, Structural Dynamics, and Materials Conference, 2015. doi:https://doi.org/10.2514/6.2015-0137.

[24] E. Carrera, A. Pagani, G. Silva, Global-local structural analysis of composite wings, in: 31th Congress of the International Council of the Aeronautical Sciences, 2018.
URL https://www.icas.org/ICAS_ARCHIVE/ICAS2018/data/papers/ICAS2018_0245_paper.pdf

[25] M. I. Izzi, M. Montemurro, A. Catapano, D. Fanteria, J. Pailhès, Multi-scale optimisation of thin-walled structures by considering a global/local modelling approach, Proceedings of the Institution of Mechanical Engineers, Part G : Journal of Aerospace Engineering (2020 (In Press)).

[26] M. I. Izzi, M. Montemurro, A. Catapano, J. Pailhès, A multi-scale two-level optimisation strategy integrating a global/local modelling approach for composite structures, Composite Structures 237 (2020).
URL https://doi.org/10.1016/j.compstruct.2020.111908

[27] E. Panettieri, M. Montemurro, D. Fanteria, F. Coccia, Multi-scale least-weight design of a wing-box through a global/local modeling approach, Journal of Optimization

Theory and Applications (2020).
URL https://doi.org/10.1007/s10957-020-01693-y

[28] M. Montemurro, A contribution to the development of design strategies for the optimisation of lightweight structures, Hdr thesis, Université de Bordeaux (2018).
URL http://hdl.handle.net/10985/15155

[29] M. Montemurro, A. Catapano, D. Doroszewski, A multi-scale approach for the simultaneous shape and material optimisation of sandwich panels with cellular core, Composites Part B: Engineering 91 (2016) 458 – 472.

[30] M. Montemurro, A. Catapano, A new paradigm for the optimum design of variable angle tow laminates, in: G. Buttazzo, A. Frediani (Eds.), Variational analysis and aerospace engineering: mathematical challenges for the aerospace of the future, Vol. 116 of Springer Optimization and Its Applications, Springer, New York, NY, 2016. doi:10.1007/978-3-319-45680-5.

[31] G. Costa, M. Montemurro, J. Pailhès, A general hybrid optimization strategy for curve fitting in the non-uniform rational basis spline framework, Journal of Optimization Theory and Applications 176 (1) (2018) 225 – 251.

[32] M. Montemurro, A. Catapano, On the effective integration of manufacturability constraints within the multi-scale methodology for designing variable angle-tow laminates, Composite Structures 161 (2017) 145 – 159.

[33] M. Montemurro, M. I. Izzi, J. E. Yagoubi, D. Fanteria, Least-weight composite plates with unconventional stacking sequences: Design, analysis and experiments, Journal of Composite Materials 53 (16) (2019) 2209–2227. doi:10.1177/0021998318824783.

[34] E. Panettieri, M. Montemurro, A. Catapano, Blending constraints for composite laminates in polar parameters space, Composites Part B: Engineering 168 (2019) 448–457. doi:https://doi.org/10.1016/j.compositesb.2019.03.040.

[35] M. Montemurro, A. Pagani, G. A. Fiordilino, J. Pailhès, E. Carrera, A general multi-scale two-level optimisation strategy for designing composite stiffened pan-

els, Composite Structures 201 (2018) 968 – 979. doi:https://doi.org/10.1016/j.compstruct.2018.06.119.

[36] L. Cappelli, M. Montemurro, F. Dau, L. Guillaumat, Characterisation of composite elastic properties by means of a multi-scale two-level inverse approach, Composite Structures 204 (2018) 767–777.

[37] Y. Audoux, M. Montemurro, J. Pailhès, A surrogate model based on non-uniform rational b-splines hypersurfaces, in: CIRP Procedia, Vol. 70, 2018, pp. 463–468.

[38] Y. Audoux, M. Montemurro, J. Pailhès, Non-uniform rational basis spline hyper-surfaces for metamodelling, Computer Methods in Applied Mechanics and Engineering 364 (2020).
URL https://doi.org/10.1016/j.cma.2020.112918

[39] Y. Audoux, M. Montemurro, J. Pailhès, A metamodel based on non-uniform rational basis spline hyper-surfaces for optimisation of composite structures, Composite Structures (2020).
URL https://doi.org/10.1016/j.compstruct.2020.112439

[40] A. Frediani, K. Abu Salem, M. Picchi Scardaoni, V. Cipolla, V. Binante, G. Palaia, Preliminary design of the reference prandtlplane, PARSIFAL Project Deliverable 3.2, University of Pisa (2018).
URL http://www.parsifalproject.eu/PARSIFAL_DOWNLOAD/PARSIFAL_D32.pdf

[41] K. Abu Salem, V. Binante, V. Cipolla, M. Maganzi, Parsifal project: a breakthrough innovation in air transport, Aerotec. Missili Spaz. 97 (1) (2018) 40–46. doi:https://doi.org/10.1007/BF03404764.

[42] EASA, Certification specifications and acceptable means of compliance for large aeroplanes, cs 25 amendment 22 (2018).
URL https://www.easa.europa.eu/document-library/certification-specifications/cs-25-amendment-22

[43] CERAS, Ceras-csr01: Short range reference aircraft.

URL http://ceras.ilr.rwthaachen.de/trac/wiki/CeRAS/AircraftDesigns/CSR01

[44] R. Zuddas, Sviluppo di metodi per il progetto ottimizzato di strutture alari, Master's thesis, University of Pisa, Department of Civil and Industrial Engineering, Aerospace division, (In italian) (2009).
URL https://etd.adm.unipi.it/theses/available/etd-05082009-103707/unrestricted/TESI_bkp.pdf

[45] Q. Liu, M. Jrad, S. B. Mulani, R. K. Kapania, Global/local optimization of aircraft wing using parallel processing, AIAA Journal 54 (11) (2016) 3338–3348. doi:doi:10.2514/1.j054499.

[46] B. K. Stanford, P. D. Dunning, Optimal topology of aircraft rib and spar structures under aeroelastic loads, Journal of Aircraft 52 (4) (2015) 1298–1311. doi:https://doi.org/10.2514/1.C032913.

[47] U. G. Goranson, Fatigue issues in aircraft maintenance and repairs, International Journal of Fatigue 20 (6) (1998) 413–431. doi:doi:10.1016/s0142-1123(97)00029-7.

[48] D. Longchao, C. Hang, Z. Yuntao, W. Xinwei, F. Xue, B. Yixiang, Y. Gang, An extended method of estimating the fatigue performance of mechanical structures with fasteners subject to shear loads, Advances in Mechanical Engineering 10 (4) (2018). doi:10.1177/1687814018767716.

[49] An., Federal register, aging airplane program: Widespread fatigue damage, Tech. Rep. 219, Department of Transportation, Federal Aviation Administration (2010).
URL https://www.govinfo.gov/content/pkg/FR-2010-11-15/pdf/2010-28363.pdf

[50] An., Statistical loads data for the airbus a-320 aircraft in commercial operations, Tech. Rep. DOT/FAA/AR-02/35, U.S. Department of Transportation, Federal Aviation Administration (2012).
URL http://www.tc.faa.gov/its/worldpac/techrpt/ar02-35.pdf

[51] M. Miner, Cumulative damage in fatigue, J Appl Mech 3 (1945) 159–163.

[52] E. Rizzo, Optimization methods applied to the preliminary design of innovative, non conventional aircraft configurations, Ph.D. thesis, University of Pisa, Department of Civil and Industrial Engineering, Aerospace division (2007).

[53] E. Rizzo, A. Frediani, Application of optimisation algorithms to aircraft aerodynamics, in: G. Buttazzo, A. Frediani (Eds.), Variational Analysis and Aerospace Engineering, Vol. 33 of Springer Optimization and Its Applications, Springer, New York, NY, 2009. doi:https://doi.org/10.1007/978-0-387-95857-6_23.

[54] M. Drela, H. Youngren, Avl overwiew (2013).
URL http://web.mit.edu/drela/Public/web/avl/

[55] V. Cipolla, A. Frediani, K. Abu Salem, V. Binante, E. Rizzo, M. Maganzi, Preliminary transonic cfd analyses of a prandtlplane transport aircraft, in: Transportation Research Procedia, Vol. 29, 2018, pp. 82–91. doi:https://doi.org/10.1016/j.trpro.2018.02.008.

[56] A. Frediani, V. Cipolla, K. Abu Salem, V. Binante, M. Picchi Scardaoni, Conceptual design of prandtlplane civil transport aircraft, Proceedings of the Institution of Mechanical Engineers, Part G: Journal of Aerospace Engineering (2019). doi:https://doi.org/10.1177/0954410019826435.

[57] M. C. Y. Niu, Airframe Structural Design, Conmilit Press Ltd., Hong Kong, 1988.

[58] G. Bertolino, M. Montemurro, G. De Pasquale, Multi-scale shape optimisation of lattice structures : an evolutionary-based approach, International Journal on Interactive Design and Manufacturing 13 (4) (2019) 1565–1578.

[59] L. Cappelli, G. Balokas, M. Montemurro, F. Dau, L. Guillaumat, Multi-scale identification of the elastic properties variability for composite materials through a hybrid optimisation strategy, Composites Part B : Engineering (2019).
URL https://doi.org/10.1016/j.compositesb.2019.107193

[60] J. R. Vinson, R. L. Sierakowski, The behavior of structures composed of composite materials, Springer, Dordrecht, 2008.

[61] A. W. Leissa, Buckling of laminated composite plates and shell panels, Final Report AFWAL-TR-85-3069, Air Force Wright Aeronautical Laboratories (1985).

[62] Y. Narita, A. W. Leissa, Buckling studies for simply supported symmetrically laminated rectangular plates, International Journal of Mechanical Sciences 32 (11) (1990) 909–924. doi:10.1016/0020-7403(90)90063-o.

[63] M. Montemurro, A. Vincenti, P. Vannucci., The Automatic Dynamic Penalisation method (ADP) for handling constraints with genetic algorithms, Computer Methods in Applied Mechanics and Engineering 256 (2013) 70–87.